Local mean-field study of capillary condensation in silica aerogels

F. Detcheverry, E. Kierlik, M. L. Rosinberg, and G. Tarjus
Laboratoire de Physique Théorique des Liquides, Université Pierre et Marie Curie, 4 place Jussieu, 75252 Paris Cedex 05, France
(Received 10 June 2003; published 17 December 2003)

We apply local mean-field (i.e., density functional) theory to a lattice model of a fluid in contact with a dilute, disordered gel network. The gel structure is described by a diffusion-limited cluster aggregation model. We focus on the influence of porosity on both the hysteretic and the equilibrium behavior of the fluid as one varies the chemical potential at low temperature. We show that the shape of the hysteresis loop changes from smooth to rectangular as the porosity increases and that this change is associated with disorder-induced out-of-equilibrium phase transitions that differ in adsorption and in desorption. Our results provide insight in the behavior of ^{4}He in silica aerogels.

DOI: 10.1103/PhysRevE.68.061504 PACS number(s): 64.70.Fx, 64.60.−i, 75.60.Ej

I. INTRODUCTION

The influence of quenched disorder on phase transitions and critical phenomena continues to be the focus of intensive experimental and theoretical research activity. Major effects are expected and actually observed when the disorder couples linearly to the order parameter of the system, a situation that is realized when a fluid or a fluid mixture is confined within a porous glass or is in contact with the interconnected strands of a gel. A dilute rigid network is a particularly interesting medium from a theoretical perspective because exclusion (i.e., confinement) effects do not play a dominant role, so that the random-field Ising model (RFIM) may be a useful framework to interpret the experimental observations [1].

A striking example of the influence of a gel network on fluid phase behavior is provided by the thermodynamic studies of Chan and co-workers on ^{4}He in silica aerogels of varying porosity. Silica aerogels are highly porous, fractal-like solids made of a tenuous network of SiO_2 strands interconnected at random sites. In a 95% porosity aerogel, specific heat and adsorption (vapor-pressure isotherm) measurements [2] performed in the vicinity of the critical temperature of the pure fluid ($T_c = 5.195$ K) show evidence of a phase separation between a low-density ''vapor'' phase (presumably composed of ^{4}He vapor plus a liquid film around the silica strands [3]) and a high-density ''liquid'' phase filling the whole pore space. The first-order transition appears to terminate at a sharply defined critical point that is only 31 mK below T_c, which suggests that the system is in a weak random-field regime. The coexistence boundary in the presence of aerogel is, however, much narrower than in the pure system. Subsequently, similar results were obtained with N_2 in the same aerogel, using light scattering and vapor-pressure isotherms [4]. Since out-of-equilibrium and hysteretic effects due to domain formation are generally observed in random-field systems below the critical temperature of the pure system (as illustrated by the behavior of binary mixtures in aerogels [5] and diluted antiferromagnets in a magnetic field [6]), it is noteworthy that no hysteresis is present in the measurements performed in Refs. [2,4]. The gel-fluid system has thus reached equilibrium within the time scale of the experiments, which is indeed found much longer than the characteristic time of activated dynamics [4]. The situation changes, however, at lower temperatures and the adsorption of ^{4}He in a 98% porosity aerogel is clearly hysteretic at 3.60 K and 2.34 K [7,8]. Both adsorption and desorption isotherms display a vertical step at well-defined pressures, but draining occurs at a lower pressure than filling [9]. The shape of the hysteresis loop, moreover, depends on the porosity of the aerogel: in an aerogel of 87% porosity, ^{4}He adsorbs and desorbs gradually at 2.42 K and there is no signature of a ''liquid-vapor'' phase coexistence [see Fig. 4(c) in Ref. [8]]. Such hysteretic behavior is reminiscent of capillary condensation in a low-porosity solidlike Vycor glass where one observes a rapid increase of the adsorbed quantity at a pressure below the bulk saturated vapor pressure, but no sharp vertical step in the adsorption isotherms [10]. The mechanism for hysteresis in porous substrates has prompted much discussion in the literature and various explanations have been proposed, focusing either on single-pore metastability of the van der Waals type or on network pore-blocking effects [11]. Since both models seem completely inadequate to describe light aerogels, the ^{4}He experiments raise several questions: what is the scenario for the change in the shape of the hysteresis loops [12]? Do filling and draining obey different mechanisms? What is the true equilibrium behavior when hysteresis is present?

These questions are addressed in the present work where we build on our earlier studies of capillary condensation in disordered porous solids [13–15], but focusing on aerogels. We are mainly interested in the influence of the porosity on the hysteretic behavior of sorption isotherms. This is partly motivated by theoretical studies of the zero-temperature RFIM which predict the existence of a disorder-induced out-of-equilibrium phase transition in the hysteresis loop [16]. The first experimental observations of this phase transition have been recently reported in the literature [17], and we argue that the change in the ^{4}He adsorption isotherm from sharp to smooth can be interpreted within the same framework. We propose a different scenario for draining and we relate the observed behavior to an out-of-equilibrium phase transition associated with the depinning of the liquid-vapor interface. The approach we develop is similar to that used previously for calculating the irreversible behavior of spin glasses, random-field ferromagnets, and diluted antiferro-

magnets [18]; it consists in studying the evolution of the free-energy surface (more precisely, the grand-potential surface Ω) as the external driving field (here, the pressure P of the external vapor or, equivalently, the chemical potential μ) is changed. Ω is a functional of the local fluid density and is treated in the mean-field approximation. At low temperatures this multidimensional free-energy landscape is characterized by a large number of local minima in which the system may be trapped. The main physical assumption underlying our description is that thermally activated processes play a negligible role on the time scale of the experiments (in other words, the dynamics is similar to that at $T=0$). The evolution of the system then proceeds either continuously by the deformation of the local minimum in which the system is trapped or when this latter becomes unstable by a jump to another minimum (avalanche); the response to the driving field is then discontinuous and irreversible. Since it is impossible to perform such a study for a continuous model because of computational limitations (especially when finite-size scaling analysis is required near phase transitions), we adopt a lattice-gas description that incorporates at a coarse-grained level the geometric and energetic disorder of the gel-fluid mixture [19]. Previous work has shown that many of the phenomena observed in experiments on fluids in disordered porous solids can be reproduced qualitatively by such simple lattice models [13–15,20]. As in other studies of phase transitions in aerogel [21,22], we model the solid by a fractal structure obtained by diffusion-limited cluster-cluster aggregation.

The paper is organized as follows. In Sec. II, we introduce the lattice model and discuss some important features of the aerogel structure. In Sec. III, we present the local mean-field theory and describe the numerical procedure. The results for the adsorption, desorption, and equilibrium isotherms in 87% and 95% porosity aerogels at $T/T_c=0.45$ are given in Sec. IV. The final section presents a summary and conclusion.

II. LATTICE MODEL AND AEROGEL STRUCTURE

The lattice model used in this work describes the solid as a collection of fixed impurities that exert a random yet correlated (by the connectivity of the strands) external field on the atoms of the fluid. The Hamiltonian is given by [23,24]

$$\mathcal{H}=-w_{ff}\sum_{\langle ij\rangle}\tau_i\tau_j\eta_i\eta_j-\mu\sum_i\tau_i\eta_i$$

$$-w_{sf}\sum_{\langle ij\rangle}[\tau_i\eta_i(1-\eta_j)+\tau_j\eta_j(1-\eta_i)], \qquad (1)$$

where $\tau_i=0,1$ is the usual fluid occupation variable ($i=1,\ldots,N$) and $\eta_i=1,0$ is a quenched random variable that characterizes the presence of gel particles on the lattice (when $\eta_i=0$, site i is occupied by the gel); w_{ff} and w_{sf} denote, respectively, the fluid-fluid and solid-fluid attractive interactions, μ is the fluid chemical potential, and the double summations run over all distinct pairs of nearest-neighbor (nn) sites. One can thus vary the gel porosity, $p=(1/N)\Sigma_i\eta_i$, by changing the number of solid sites or modify the "wettability" of the solid surface by changing the ratio $y=w_{sf}/w_{ff}$. For $y=1/2$, the model reduces to a site diluted Ising model, as can be seen by transforming the fluid occupation variable τ_i to an Ising spin variable, $s_i=2\tau_i-1$ [24]: preferential adsorption of the liquid phase onto the gel is thus modeled by $y>1/2$. Random fields are generated in the system when $y\neq 1/2$, and the fluctuating part of the field acting on spin s_i is proportional to the number of solid particles that occupy the nearest neighbors of site i [24]. This a discrete random variable that can take the values $0,1,\ldots,c$, where c is the coordination number of the lattice, and whose probability distribution is strongly porosity dependent.

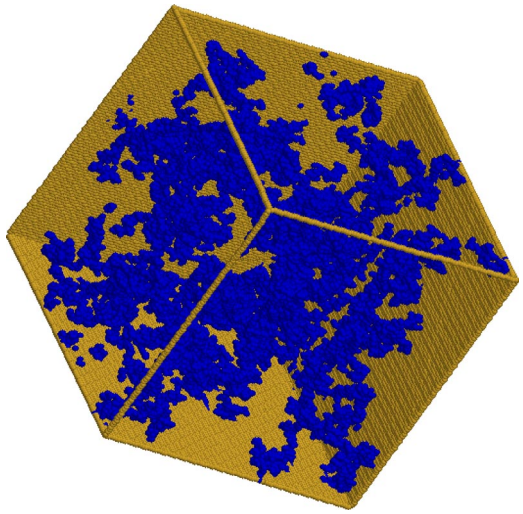

FIG. 1. Three-dimensional realization of a 98% porosity DLCA aerogel on a bcc lattice of size $L=100$ with periodic boundary conditions.

Gel configurations (i.e., sets $\{\eta_i\}$) are generated by a standard on-lattice diffusion-limited cluster-cluster aggregation (DLCA) algorithm [25] adapted to a body-centered-cubic (bcc) lattice with periodic boundary conditions. The choice of the bcc lattice will be motivated in Sec. IV B. The DLCA algorithm mimics the growth process of base-catalyzed aerogels used in helium experiments, and it has been shown to reproduce the main structural features of these aerogels measured from scattering experiments [26]. A typical example of a 98% porosity DLCA aerogel on a lattice of linear size $L=100$ is shown in Fig. 1 (from now on, we take the lattice constant a as the unit length; the total number of sites in the lattice is thus $N=2L^3$). One can clearly see the fractal-like character of the gel network that results from the aggregation mechanism.

More quantitative information on the structural properties of the gel can be extracted from the two-point correlation function $g(r)$. Each curve shown in Fig. 2 corresponds to a different porosity p and results from an average over several simulations in a box of size $L=100$ (for $p=0.87$, 0.92, 0.95) or $L=200$ (for $p=0.97$,0.98,0.99). Only the most dilute samples exhibit a true intermediate regime described by the power-law behavior $g(r)\simeq r^{-(3-d_f)}$ revealing the fractal character of the intracluster density-density correlations [27]. For $p=0.99$, one finds $d_f\approx 1.87$, a value that lies in the range 1.7–1.9 expected for DLCA in three dimensions. Note,

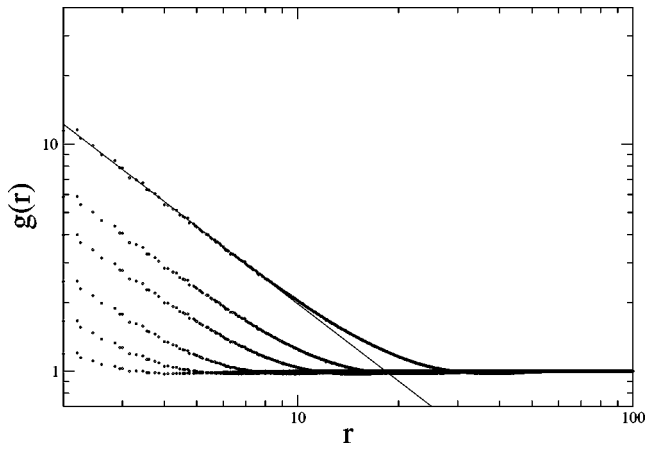

FIG. 2. Log-log plot of the aerogel correlation function $g(r)$ for $p=0.99$, 0.98, 0.97, 0.95, 0.92, and 0.87 (from top to bottom). The solid line is a fit with slope -1.13 that corresponds to the fractal regime for $p=0.99$ (the unit length is the lattice constant a).

however, that the fractal dimension decreases with increasing porosity [28], so that the asymptotic value must be somewhat smaller. Another estimation of d_f can be obtained from the average cluster size ξ_G by assuming that ξ_G varies as $\rho_G^{-1/(3-d_f)}$, where $\rho_G=1-p$ is the gel concentration. As suggested in Ref. [26], ξ_G can be estimated from the location of the first minimum of $g(r)$ (which is hardly visible on the scale of Fig. 2). The plot of ξ_G versus ρ_G shown in Fig. 3 yields $d_f \approx 1.85$. Since the correlation length is in the range 650–1300 Å for a 98% base-catalyzed aerogel [3,29] and $\xi_G(\rho_G=0.02)\approx 21$ in the simulation, one can estimate that the lattice constant a corresponds to about 30–60 Å. This is consistent with the coarse-grained picture of a gel site representing a SiO_2 particle with a diameter of about 30 Å.

Another relevant length scale is the size of the largest cavity in the aerogel [30]. Figure 4 shows the distribution $P(n)$ of nearest distances n from an empty site to the aerogel as a function of porosity (the integer ''distance'' n is defined

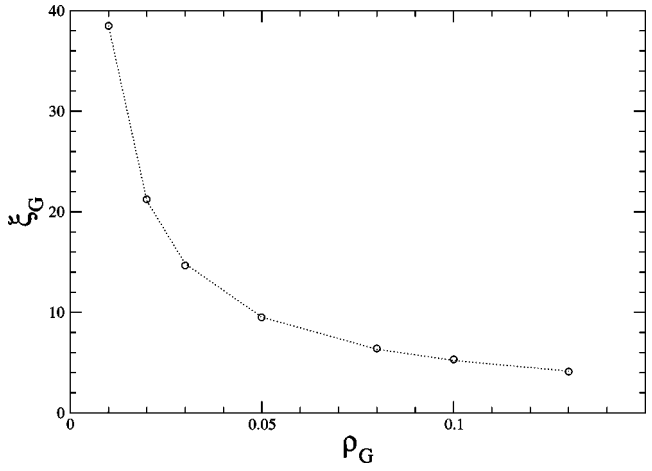

FIG. 3. Average cluster size ξ_G [estimated from the location of the first minimum of $g(r)$] as a function of the gel concentration $\rho_G=1-p$. The dashed line corresponds to the power-law fit $\xi_G=0.707\rho_G^{-0.868}$.

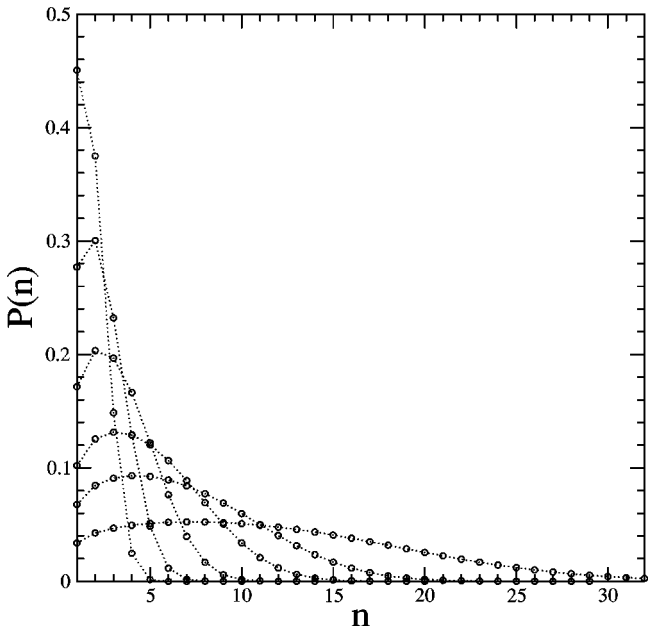

FIG. 4. Distribution $P(n)$ of nearest distances from an empty site to the gel (see the text). From right to left: $p=0.99$, 0.98, 0.97, 0.95, 0.92,0.87 (the dashed lines are guides to the eye).

here as the length of the shortest path on the lattice from an empty site to a gel site; $n=1$ means that the empty site is nn of a gel site). The plot is the normalized histogram of these distances and $\Sigma_1^n P(n')$ gives the probability of being closer than n to the aerogel. One can see that the size of the largest cavity is $n\approx 32$ for a 99% aerogel and decreases to $n\approx 10$ for a 95% aerogel and to $n\approx 5$ for a 87% aerogel. It is noticeable that the distribution changes significantly when decreasing the porosity from 95% to 87%. In the former case, $P(n)$ has its maximum at $n=2$ and there is a significant proportion of empty sites that are not in the immediate vicinity of the gel. In the latter case, $P(n)$ is monotonic and strongly peaked at $n=1$, which indicates that most of the empty sites are very close to the gel. We shall see in Sec. IV A that these differences have important implications on the behavior of the fluid during adsorption.

It is clear from Fig. 3 that the minimum system size necessary to describe correctly collective effects occurring inside the aerogel on long length scales (such as a sharp condensation event in the *whole* pore space) depends strongly on the porosity. For instance, a box of linear size $L=100$ is not large enough to represent the whole pore space of a 99% aerogel because it does not contain a sufficient number of connected fractal aggregates (a problem that cannot be cured by merely increasing the number of realizations). Within the framework of local mean-field theory, it is however impossible to simulate much larger lattices because the computational time and the memory storage requirement become prohibitive (at finite temperature, the local fluid densities are continuous variables, which forbids the use of bits algorithms). In the present work, we consider 95% and 87% aerogels for which we can investigate the statistics of collective events while working with lattices of reasonable size (between $L=25$ and $L=100$).

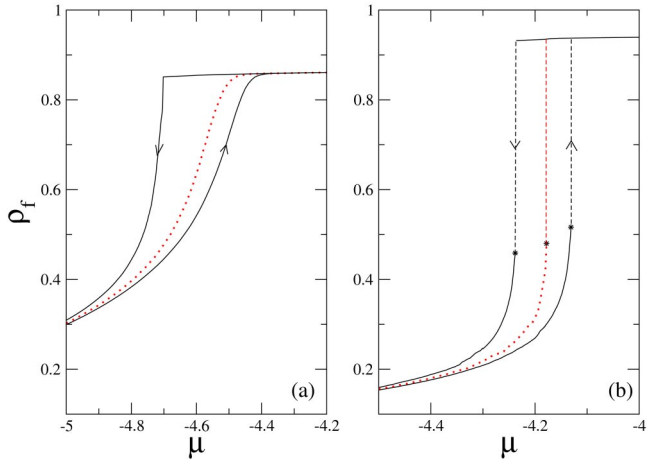

FIG. 5. Hysteresis loops in the 87% (a) and 95% (b) model aerogels calculated at $T/T_c=0.45$. Equilibrium isotherms are indicated by the dotted lines (w_{ff} is taken as the energy unit).

Since it has been shown previously that the interface between the porous solid and the bulk gas may have a dramatic effect on the desorption process [15], two different setups are considered. In the first one, the system is periodically replicated in all directions so that no interfacial effects are taken into account. In the second setup an interface is created by placing a slab of vapor of width $L_b=10$ (the gas ''reservoir'') in contact with one of the [100] faces of the simulation box. Periodic boundary conditions are then imposed in the y and z directions and reflective boundary conditions in the x direction (obtained by reflecting the lattice at the boundaries).

In order to completely specify the model, one must also fix the value of the interaction parameter y. As shown previously [15], the shape of the hysteresis loops changes with y. Since it is meaningless in a coarse-grained picture to compute y from the actual values of the fluid-fluid and solid-fluid van der Waals interactions, we have chosen its value so as to reproduce approximately the height of the hysteresis loop in the 87% aerogel at low temperature. Specifically, the results presented in this work are calculated with $y=2$, a value for which the filling of the 87% aerogel at the lower closure point of the hysteresis loop is roughly the same as in the experiment at $T=2.42$ K (i.e., at $T/T_c\approx 0.45$). This corresponds to about 1/3 of the filling reached at the plateau just before saturation, as can be seen in Fig. 4(c) of Ref. [8] [see also Fig. 5(a) below]. All calculations are done at this single reduced temperature (recall that $kT_c/w_{ff}=c/4=2$ in the mean-field approximation).

III. LOCAL MEAN-FIELD THEORY (LMFT) AND NUMERICAL PROCEDURE

For the present model, the LMFT consists in solving the self-consistent equations for the thermally averaged fluid densities $\rho_i(\{\eta_i\})=\langle \tau_i \eta_i \rangle_T$ obtained from minimizing the mean-field grand-potential functional [13]

$$\Omega(\{\rho_i\})=k_BT\sum_i [\rho_i \ln\rho_i+(\eta_i-\rho_i)\ln(\eta_i-\rho_i)] - w_{ff}\sum_{\langle ij\rangle}\rho_i\rho_j-\mu\sum_i \rho_i - w_{sf}\sum_{\langle ij\rangle}[\rho_i(1-\eta_j)+\rho_j(1-\eta_i)]. \quad (2)$$

The variational procedure $\delta\Omega/\delta\rho_i=0$ gives a set of N coupled nonlinear equations

$$\rho_i=\frac{\eta_i}{1+\exp\left[-\beta\left(\mu+w_{ff}\sum_{j/i}[\rho_j+y(1-\eta_j)]\right)\right]}, \quad (3)$$

where $\beta=1/(k_BT)$ and the sum runs over the c nearest neighbors of site i. At low temperature, these equations may have several solutions, and the grand potential corresponding to solution $\{\rho_i^\alpha\}$ is given by [14]

$$\Omega^\alpha=k_BT\sum_i \eta_i \ln\left(1-\frac{\rho_i^\alpha}{\eta_i}\right)+w_{ff}\sum_{\langle ij\rangle}\rho_i^\alpha\rho_j^\alpha. \quad (4)$$

By using an iterative method to solve Eqs. (3), one only finds solutions that are only local minima of the grand-potential surface, i.e., metastable states [18].

For a given realization of the aerogel, the sorption isotherms [i.e., the curves $\rho_f=(1/N)\Sigma_i\rho_i(\{\eta_i\},\mu)$] are obtained by increasing or decreasing the chemical potential in small steps $\delta\mu$. At each subsequent μ, the converged solution at $\mu-\delta\mu$ (on adsorption) or at $\mu+\delta\mu$ (on desorption) is used to start the iterations. The isotherms are then averaged over a number of gel realizations depending on the system size. In order to determine the equilibrium isotherms, we have also searched for additional solutions of Eqs. (3) inside the hysteresis loop by performing scanning trajectories, as explained below in Sec. IV C.

To accelerate the convergence of the numerical procedure, we have introduced the following two modifications in the iteration algorithm. First, the local densities ρ_i are updated during each iteration step, i.e., the new value of ρ_i is substituted into the right hand side of Eqs. (3) before waiting for the rotation through the indices i to be completed. Second, at each iteration step, fluid sites are sorted into two groups, ''active'' and ''passive,'' according to the relative change in the local density. At the beginning of the calculation, all sites are active and the procedure stops when all sites are passive. At each iteration only active sites are considered and their new density is calculated using Eqs. (3). If $|\rho_i^{(n)}-\rho_i^{(n-1)}|/\rho_i^{(n-1)}<10^{-6}$, where n denotes the nth iteration, the site i becomes passive; otherwise it remains active and its nearest neighbors become (or remain) active (some sites can thus be passive during a few iterations and become active again).

The advantage of this algorithm is that the number of active sites may quickly become a small fraction of the total number of sites, which of course significantly reduces the overall computation time. For instance, the number of active

sites is only $O(L^2)$ when a planar liquid-vapor interface propagates through the system. We have checked that the numerical results are not different (to the precision of the calculations) from those obtained without updating or with using a more standard convergence criterion, such as in our previous studies of fluid adsorption in random matrices [13–15]. Convergence (to an accuracy of 10^{-6}) typically requires between 10^2 and 10^3 iterations, and several CPU hours on a 2.4 GHz workstation are needed to calculate a single adsorption isotherm in a system of linear size $L=100$ (using a step $\delta\mu/w_{ff}=10^{-2}$ or 10^{-3} to increment the chemical potential). The search for equilibrium isotherms is much more time consuming (see below in Sec. IV C) and has been made possible by using parallel computation on a Beowulf cluster of 24 processors.

IV. RESULTS AND DISCUSSION

The results of the present study are summarized in Fig. 5 that shows the adsorption, desorption, and equilibrium isotherms calculated for the 87% and 95% model aerogels for $y=2$ and $T/T_c=0.45$ (from now on, μ is in units of w_{ff}, the fluid-fluid interaction parameter). These curves result from the detailed numerical analysis described in the following and correspond to the thermodynamic limit. The most striking feature is the change in the shape of the hysteresis loop from smooth to rectangular as the porosity increases. This change is similar to that observed experimentally by Chan and co-workers [see Figs. 4(b) and 4(c) in Ref. [8]]. As is explained below, we predict that the three isotherms (adsorption, desorption, and equilibrium) are discontinuous in the 95% aerogel (at least within mean-field theory where thermal fluctuations are neglected). The underlying physical mechanisms are, however, quite different.

A. Adsorption

We first examine the adsorption process. Calculations performed in the presence and in the absence of a gel/reservoir interface yield isotherms that are almost indistinguishable (except for the smallest system sizes), confirming the conclusion reached in our previous work [15] that adsorption does not depend on the existence of a free surface. This is also in line with the results of previous calculations done in single slitlike or cylindrical pores [31].

In Figs. 6(a) and 6(b) are shown some adsorption isotherms calculated in 87% and 95% porosity samples of linear size $L=50$ and $L=100$, respectively (this corresponds to roughly the same ratio $L/\xi_G\approx 10$). In both cases, we focus on the region where the adsorption is the steepest (see Fig. 5). At lower coverages, the isotherms look gradual and smooth in the two systems, but as μ increases, they consist of little steps of varying sizes. In the 87% aerogel, the size of these ''avalanches'' remains small all the way up to the slowly increasing plateau that extends to saturation. On the other hand, in the 95% aerogel, the size of the jumps tends to increase with μ and in most of the samples there is a large final avalanche after which the filling is almost complete [there are however some rare realizations where the last jump is not much larger than the preceding ones, as illustrated by one of the isotherms in Fig. 6(b)].

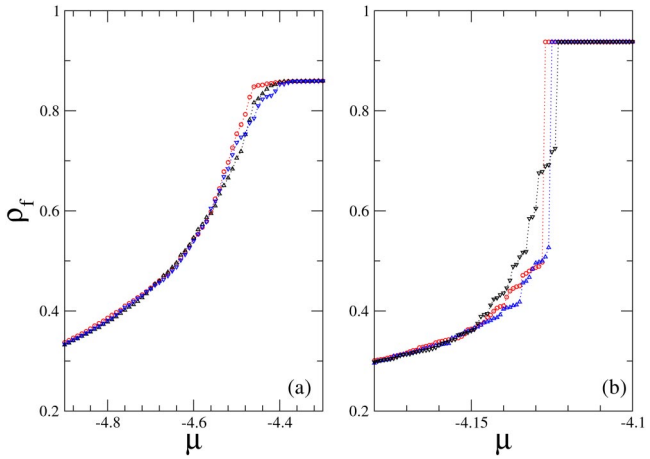

FIG. 6. Representative adsorption isotherms in 87% (a) and 95% (b) aerogels. System sizes are $L=50$ (a) and $L=100$ (b). Notice the change in the scale of the x axis between the two figures.

In order to better visualize the underlying microscopic mechanism, we show in Figs. 7 and 8 some cross sections of typical 87% and 95% porosity samples for different values of the chemical potential along the isotherms (here, the size of both systems is $L=100$). One can see that in both aerogels the first stage of the adsorption process is the formation of a liquid layer that coats the aerogel strands. Then, as μ increases, the film thickens and condensation occurs in the smallest crevices defined by neighboring gel strands. In the 87% aerogel, it is difficult to discriminate between these two filling processes because the available empty space is small, as illustrated by Fig. 4. For the same reason, the vapor bubbles that remain in the system at $\mu=-4.5$ are isolated,

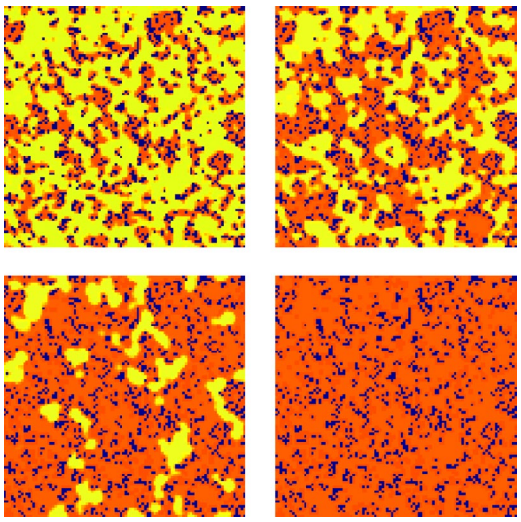

FIG. 7. Cross section of a 87% aerogel sample on adsorption at $\mu=-5$, -4.64, -4.5, and -4.35 ($L=100$). Gel sites are shown in black and fluid density is shown as various degrees of gray (or red in the online version). As explained in the text, one can actually distinguish only two regions corresponding, respectively, to $\rho_i \leqslant 0.05$ [light gray] and $\rho_i \geqslant 0.95$ [dark gray].

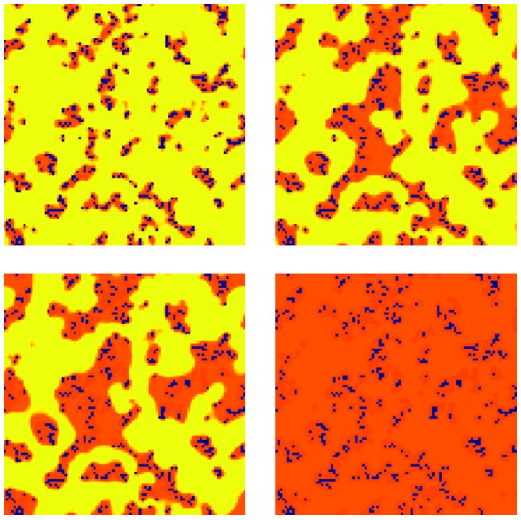

FIG. 8. Same as Fig. 7 for a 95% sample at $\mu=-4.5$, -4.16, -4.13, and -4.125 ($L=100$). This is one of the samples shown in Fig. 5(b).

and, as they shrink in size, the adsorption continues gradually until the solid is completely filled with liquid. This is precisely the scenario described in Ref. [8] from the experimental observations with ^{4}He. This is also similar to what happens in a low-porosity glass such as Vycor [32]. On the contrary, in the 95% sample, one clearly distinguishes the small capillary condensation events that occur in some regions of the aerogels (compare the figures for $\mu=-4.16$ and $\mu=-4.13$) and the major final event that corresponds to the filling of a large void space spanning the whole sample (as μ is increased from -4.13 to -4.125). Note that the local liquid-vapor interfaces inside the gel are very sharp at this low temperature, which explains why one can only distinguishes two different regions in Figs. 7 and 8. Indeed, as illustrated in Fig. 9 for the lighter aerogel, it is found that the distribution of ρ_i's is bimodal, with most of the fluid sites having a density lower than 0.05 or larger than 0.95 (the distribution is similar in the 87% porosity aerogel with just a little more intermediate densities).

From these results (see, for instance, the cross section of the 95% aerogel at $\mu=-4.13$), there is no indication that the radius of curvature of the liquid-vapor interface is concave and uniform throughout the sample just before the major condensation event, as was suggested in Ref. [8]. This makes unlikely any interpretation in terms of a traditional capillary condensation model based, for instance, on the application of the Kelvin equation [3,33]. Indeed, condensation in the remaining void space is itself triggered by a condensation event that occurs in one (or several) small region of the aerogel and that induces further condensation in the system. This collective behavior in the form of avalanches of varying sizes is similar to that of the Gaussian RFIM at $T=0$ proposed by Sethna and co-workers to describe the Barkhausen effect in low-T ferromagnetic materials [16]. Increasing slowly the chemical potential of the adsorbed fluid is equivalent to increasing adiabatically the applied field in a ferromagnet, and changing the porosity of the aerogel modifies the amount of quenched disorder in the system. In the

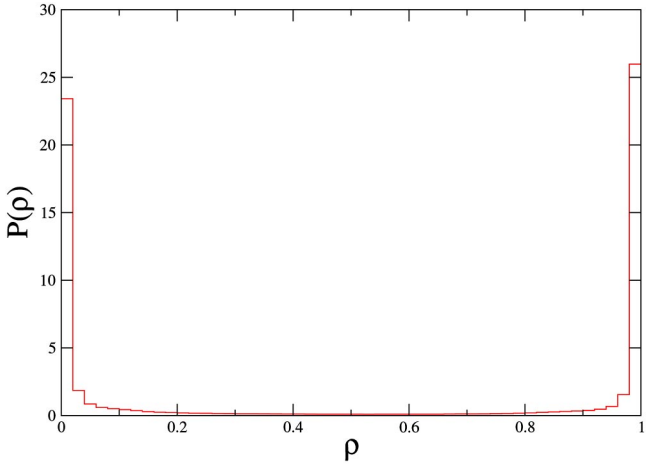

FIG. 9. Histogram of the local fluid densities ρ_i in the 95% aerogel sample of Fig. 8 at $\mu=-4.13$.

RFIM, the amount of disorder is controlled by the width of the random-field distribution: only small avalanches are observed for large disorder, resulting in a smooth hysteresis loop, whereas one macroscopic avalanche produces a discontinuity in the magnetization for small disorder [16,34]. The transition between these two regimes for a certain value of the disorder corresponds to a critical out-of-equilibrium phase transition at which the distribution of avalanches follows a power law.

The existence of a major condensation event in most of the 95% samples of size $L=100$ therefore suggests that there is one macroscopic (i.e., infinite) avalanche in the thermodynamic limit, corresponding to a finite jump in the adsorption isotherm. However, this can be only confirmed by performing a finite-size scaling analysis of the isotherms obtained after averaging over many gel realizations. We indeed observe significant sample-to-sample fluctuations both in the location and the height of the largest jump. Such average isotherms are shown in Fig. 10. For the 87% aerogel, there is

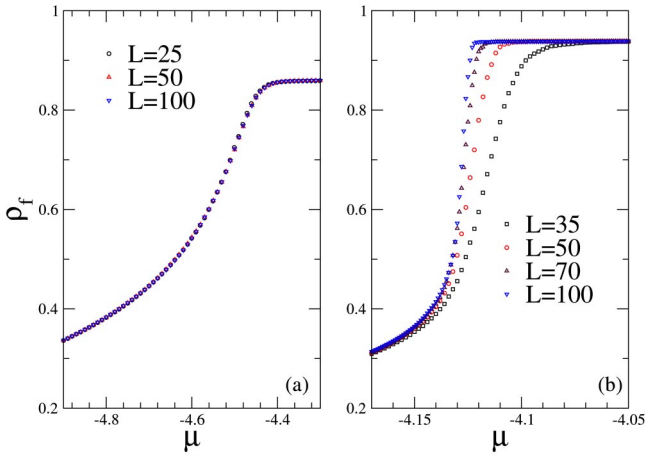

FIG. 10. Average adsorption isotherms in 87% (a) and 95% (b) aerogels for different system sizes. The number of gel realizations ranges from 500 ($L=35$) to 20 ($L=100$) for the 87% aerogel and from 2000 ($L=35$) to 300 ($L=100$) for the 95% aerogel.

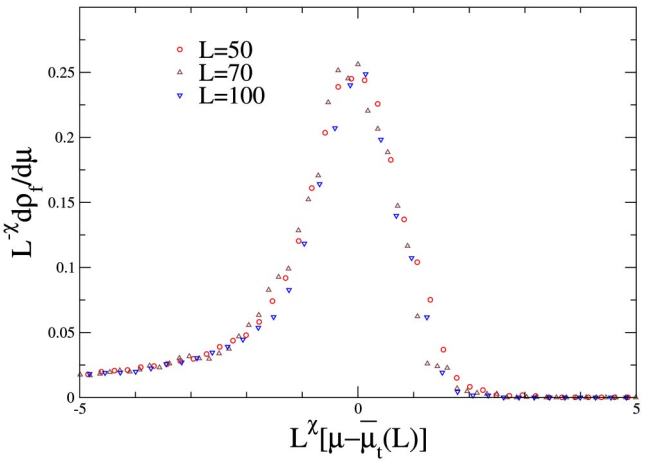

FIG. 11. Scaling plot of the compressibility curves $d\rho_f/d\mu$ during adsorption in the 95% aerogel with $\chi=1.22$ [$\bar{\mu}_t(L)=-4.123$, -4.126, and -4.128 for $L=50$, 70, and 100, respectively; extrapolation to $L\to\infty$ gives $\mu_t=\lim_{L\to\infty}\bar{\mu}_t(L)\simeq-4.131$].

obviously no size dependence and we can safely conclude that the adsorption is gradual in the thermodynamic limit. On the contrary, in the lighter aerogel, the isotherms look steeper and steeper as the system size is increased and the results suggest that there is indeed a discontinuity when $L\to\infty$ (the isotherm corresponding to $L=35$ is shown here for completeness, but this size is probably too small to describe properly a 95% aerogel). As we discussed elsewhere [14] in the case of fluid equilibrium behavior in purely random solids, one expects that the maximal slope of the isotherms should scale as $L^{3/2}$ at a first-order transition [assuming that the location of the largest jump fluctuates around its mean value $\bar{\mu}_t(L)$ with a variance $\delta\mu_t(L)^2\propto L^{-3}$]. As shown in Fig. 11, one can obtain a reasonably good collapse of the $L=50$, 70, and 100 irreversible ''compressibility'' curves $d\rho_f/d\mu$ by using the scaling variable $L^{\chi}\{\mu-\bar{\mu}_t(L)\}$ with $\chi\approx1.22$.

There are at least two possible explanations for the discrepancy with the expected value $\chi=3/2$. First, the system sizes could still be too small so that too many gel realizations would have a nontypical behavior, with several avalanches of similar heights (note that in a coarse-grained picture of a 95% gel-fluid system where a region of size ξ_G is represented by a single effective spin, there would be only about 10^3 such effective spins in a sample of size $L=100$). Second, one may be close to the critical value p_c of the disorder, i.e., the critical value of the porosity for $y=2$ and $T/T_c=0.45$, for which the infinite avalanche first appears. Studies of the $T=0$ RFIM have shown, moreover, that the critical region is unusually large [16]. The value $\chi=1.22$ is compatible with the predictions of Sethna and co-workers, with $\chi=\beta\delta/\nu\simeq2-\eta$ [35], although one cannot also exclude that the exponents differ from those of the conventional RFIM because of the presence of impurities [36]. In any case, it seems reasonable, on the basis of the present calculations, to predict the existence of a phase transition with most probably a discontinuity in the adsorption isotherm in the thermodynamic limit, as shown in Fig. 5(b).

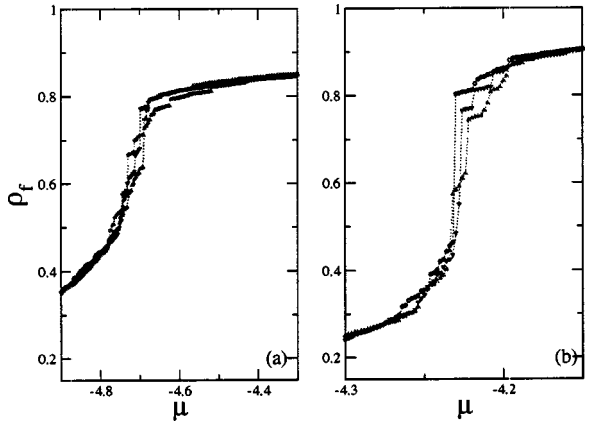

FIG. 12. Desorption isotherms in 87% (a) and 95% (b) aerogels. System sizes are $L=50$ (a) and $L=100$ (b).

B. Desorption

As discussed elsewhere [15], fluid desorption in disordered porous solids can take place via several different mechanisms, depending on the temperature and on the structural and energetic properties of the solid (in Ref. [15], however, only the influence of the interaction parameter y, i.e., of the wetting properties of the adsorbed fluid, was described). In a first mechanism, desorption is due to the appearance of vapor bubbles in the bulk of the material, bubbles that grow, coalesce, and eventually extend over the whole pore space. The mass adsorbed then decreases continuously. In the other mechanisms, draining of the solid starts from the surface, and the desorption is associated with the penetration of a vapor-liquid interface which was previously pinned by the irregularities of the solid structure for μ larger than some threshold value μ_c (the ''depinning''threshold). The desorption curve is then either gradual or discontinuous, depending on whether the growth of the vapor domain is isotropic and percolationlike (self-similar), or compact (self-affine). In those cases the transition is however always critical because the scale of the rearrangements of the interface diverges as $\mu\to\mu_c^+$. This is very similar to the physics of fluid invasion in porous media [37], although we are considering here a single compressible fluid, and of field-driven domain wall motion in disordered magnets [38].

In order to find what are the relevant mechanisms in the 87% and 95% aerogels for $y=2$ and $T/T_c=0.45$, we have studied the two systems in the presence and in the absence of the interface with the gas reservoir. In the latter case, we find that emergence of vapor bubbles in the bulk of the solid only occurs at low values of the chemical potential ($\mu\simeq-5.27$ and $\mu\simeq-5.25$ for 87% and 95% aerogels, respectively), very close to the value $\mu_{spi}=-5.249$ corresponding to the liquid (mean-field) spinodal of the bulk fluid at $T/T_c=0.45$. This shows that the perturbation induced by the solid is too small to displace significantly the liquid spinodal. On the other hand, the contact with the ambient vapor at the surface of the gel has a major influence, as illustrated in Fig. 12 by typical desorption isotherms calculated in the presence of a free surface. One can see that when decreasing the chemical potential all the curves exhibit a pronounced drop much before

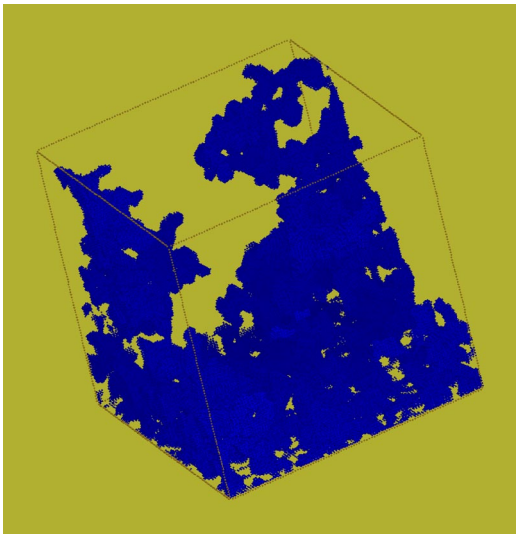

FIG. 13. Invading vapor domain V_t (in dark) in a 87% aerogel at $\mu=-4.706$ ($L=100$). 10% of the fluid has drained out. The gas reservoir located at the bottom of the box and the aerogel are not shown.

vapor bubbles appear in the bulk of the material. This is a clear indication that the mechanism of desorption is due to the surface.

The isotherms shown in Fig. 12 consist of many steps of varying size, but it also appears that one step is significantly larger than the other ones in most of the 95% samples, a feature that is not present in the isotherms of the 87% aerogel. This suggests that the growth morphology of the invading vapor domain may change with the porosity. This is confirmed by the snapshots displayed in Figs. 13 and 14 that show the invading vapor domain in two typical 87% and 95% samples when about 10% of the fluid has drained out of the aerogel. This is just after the onset of the sharp drop in the isotherms. As in the case of adsorption, we find that the distribution of ρ_i's is bimodal in this range of chemical potentials, with most of the fluid sites having a density lower

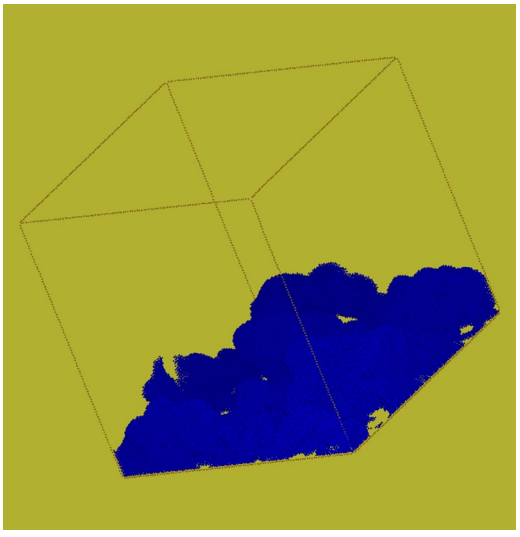

FIG. 14. Same as Fig. 13 but for a 95% aerogel at $\mu=-4.220$.

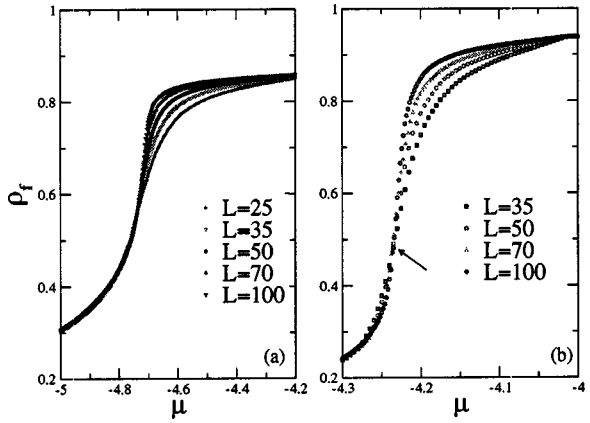

FIG. 15. Average desorption isotherms in 87% (a) and 95% (b) aerogels for different system sizes. The number of gel realizations ranges from 1000 ($L=25$) to 100 ($L=100$) for the 87% aerogel and from 1000 ($L=35$) to 200 ($L=100$) for the 95% aerogel. The arrow in (b) indicates the common intersection of the curves.

than 0.05 or larger than 0.95. One can thus identify unambiguously the emptied sites. Although the volume occupied by the vapor is the same in the two samples (about 200 000 sites), the morphology of the domain is remarkably different. In the 87% aerogel, the vapor domain exhibits an intricate isotropic structure that resembles that produced in invasion percolation. In contrast, the domain looks compact with a self-affine interface in the lighter aerogel. This is very similar to the two regimes observed in the $T=0$ RFIM when an interface separating two magnetic domains is driven by an external field [40]: when the disorder is large, the interface forms a self-similar pattern with a large-scale structure characteristic of percolation, whereas the growth is compact and the domain wall forms a self-affine fractal surface at intermediate degrees of disorder (note that the use of the body-centered cubic lattice has allowed us to suppress the faceted growth regime that is observed at $T/T_c=0.45$ in the 95% porosity aerogel on the simple cubic lattice [39]; this regime is an artifact of the lattice description).

In order to confirm the existence of two growth regimes and to determine the actual behavior in the thermodynamic limit, a finite-size scaling analysis of the desorption isotherms is required. Average isotherms calculated for different system sizes are shown in Fig. 15. By analogy with the problem of a driven interface in the $T=0$ RFIM, one expects that the total volume $V_t(\mu)$ of the invading vapor domain shows a power-law divergence at the depinning threshold μ_c. Then, assuming that the only relevant length scales near μ_c are the system size L and a single correlation length $\xi \sim[(\mu-\mu_c)/\mu_c]^{-\nu}$, the dependence of V_t on system size should be described by the scaling form $L^{D_f}g(x)$, where D_f is the fractal dimension characterizing the domain and g is a universal function of the scaling variable $x=L^{1/\nu}(\mu-\mu_c)/\mu_c$ [40].

In both aerogels, one observes important finite-size effects (see Fig. 15), but, unfortunately, they are not only due to the existence of a diverging correlation length in the system but also due to boundary effects. There is indeed an initial re-

gime in which desorption is due to the draining of large crevices at the surface of the gel where the fluid is in direct contact with the ambient vapor. For a given porosity, the number of these crevices is proportional to L^2 and the contribution to the fluid density is thus proportional to $1/L$. It turns out that this initial regime extends to rather low values of the chemical potential ($\mu \simeq -4.6$ and $\mu \simeq -4.15$ for the 87% and 95% aerogels, respectively), so that the scaling region around the depinning threshold is too small to be studied properly and to extract the values of the critical exponents (such an effect is not present in the numerical studies of domain growth in the standard $T=0$ RFIM [38] because there is a different random field on *each* site of the lattice and no equivalent of the crevices). We note, however, that the curves in Fig. 15(b) have a common intersection at $\mu \simeq -4.24$, in contrast with those in Fig. 15(a). This is consistent with the scaling ansatz for the volume of the invading vapor domain with $D_f = 3$ for the 95% aerogel and $D_f < 3$ for the 87% aerogel. We thus conclude that the desorption seems to be discontinuous in the first case and gradual (percolation-like) in the second one.

This leads to the isotherms shown in Fig. 5. Their shape resembles that of the experimental curves in Figs. 4(b) and 4(c) of Ref. [8]. The minor differences can be rationalized: the experimental isotherm in the 87% aerogel [Fig. 4(c) in Ref. [8]] does not exhibit a sharp kink at μ_c, but this rounding may be due to the activated processes that are neglected in the present treatment; Fig. 4(b) in Ref. [8] corresponds to a 98% aerogel, which probably explains why the shape of the hysteresis is more rectangular than in the present Fig. 5(b).

C. Equilibrium

In order to determine the equilibrium isotherms, one has to find, for each value of μ, the lowest lying state(s) among all the metastable states obtained from Eqs. (3). A complete enumeration of these states is, however, an impossible numerical task, and like in previous work [13,14], we have only calculated a limited number of states that, hopefully, can provide a good approximation of the equilibrium isotherm. This can be checked *a posteriori* by using the Gibbs adsorption equation $\rho_f = -\partial(\Omega/N)/\partial\mu$, which is only satisfied by the equilibrium curve [13]. In Refs. [13,14], we searched for metastable states inside the hysteresis loop by starting the iterative procedure with initial configurations corresponding to uniform fillings of the lattice (with $\rho_i^{(0)} = \rho$ varying between 0 and $1-p$). This method, however, does not converge in dilute aerogels because the structure is very inhomogeneous and correlated, at least for distances smaller than ξ_G. It is then likely that all metastable fluid configurations are also very inhomogeneous and cannot be reached iteratively from initial uniform fillings. We have thus searched for metastable states by calculating desorption and adsorption scanning curves, i.e., by performing incomplete filling or draining of the aerogel and then reversing the sign of the evolution of the chemical potential. For convenience, these (very long) calculations are done in systems with periodic boundary conditions in all directions, i.e., in the absence of an interface with the reservoir [41].

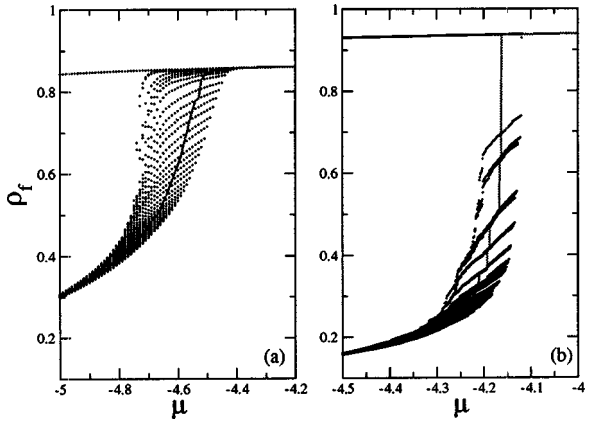

FIG. 16. Typical desorption scanning curves (points) and equilibrium isotherms (solid lines) in 87% (a) and 95% (b) aerogels ($L=70$).

Some typical desorption scanning curves are shown in Figs. 16(a) and 16(b). In both cases, the top curve is the major desorption branch, and by comparing with the isotherms shown in Figs. 12 or 15, it is clear that the part of this branch extending to low μ's and corresponding to liquidlike metastable states that are isolated from the other states is an artifact coming from the absence of the interface with the reservoir. We also notice that there are no scanning curves in the upper part of the hysteresis loop for the 95% sample. This is because there is a jump in the adsorption isotherm and, thus, there are no intermediate states from which desorption can be started. Therefore the states contained in this region of the plane (ρ_f, μ) cannot be reached by performing scanning trajectories [42]. (Further work is clearly needed to determine if there are no metastable states at all in this region or if the states can be obtained, by other means, for instance, by changing the temperature.)

Figure 16 also shows the approximate equilibrium isotherms obtained by selecting, for each value of μ, the state α that gives the lowest value of the grand potential, as calculated from Eq. (4). We have checked that taking into account the additional metastable states obtained from the adsorption scanning curves did not change significantly the results (as in Ref. [14], we have also checked that keeping all solutions with a weighting factor equal to the Boltzmann factor gives the same isotherms). As illustrated in Figs. 17(b) and 18(b), the Gibbs adsorption equation is very well verified along these curves. This indicates that we have indeed obtained a good approximation of the true equilibrium isotherms. In contrast, thermodynamic consistency is strongly violated along the adsorption and desorption branches [see Figs. 17(a) and 18(a)]. The presence of (δ) peaks in $\partial\Omega/\partial\mu$ also shows that the grand potential Ω changes discontinuously (as the fluid density ρ_f) during adsorption and desorption in a single finite sample. On the other hand, Ω is continuous (but ρ_f is discontinuous) along the equilibrium isotherm, as already noticed in Ref. [14].

One can see from Figs. 16(a) and 16(b) that the equilibrium behavior is different in the 87% and 95% porosity aero-

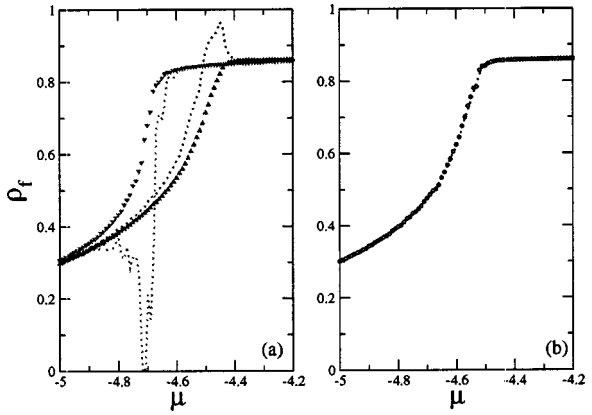

FIG. 17. Check of thermodynamic consistency along the adsorption, desorption, and equilibrium isotherms for a 87% porosity aerogel ($L=70$). (a) Adsorption and desorption and (b) equilibrium. Symbols: average fluid density ρ_f. Dashed curves: related quantity obtained by differentiating the corresponding grand potential with respect to the chemical potential.

gels. In particular, there is a large final jump in the isotherm of Fig. 16(b). The same feature exists in all samples, but in order to conclude on the actual behavior in the infinite system one has again to analyze the size dependence of the average isotherms. This is shown in Fig. 19. For the 87% aerogel, there is almost no size dependence and it is clear that no transition occurs when $L\to\infty$. On the other hand, for the 95% aerogel, the isotherms become steeper as L increases and there is a rather well defined common intersection at $\mu_t\simeq -4.17$. This is a clear indication that a phase transition does occur in the thermodynamic limit. However, we have not succeeded in obtaining a satisfactory collapse of the isotherms using the scaling reduced variable $L^{3/2}[\mu-\mu_t(L)]/\mu_t(L)$ as was done in Ref. [14] in the case of a random solid. The origin of this problem is still unclear, but we suspect that the system sizes are again too small. Indeed, we note that the maximal slope increases rather weakly between $L=35$ and $L=70$, but has a size dependence consistent with the exponent 3/2 between $L=70$ and $L=100$. We thus conclude that our results are consistent with a discontinuous jump in the thermodynamic limit, as indicated in Fig. 5(b). This corresponds to a true equilibrium liquid-vapor phase separation in the system.

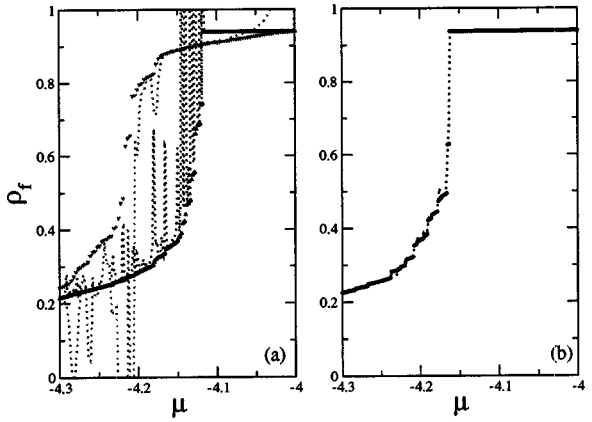

FIG. 18. Same as Fig. 17 but for a 95% aerogel.

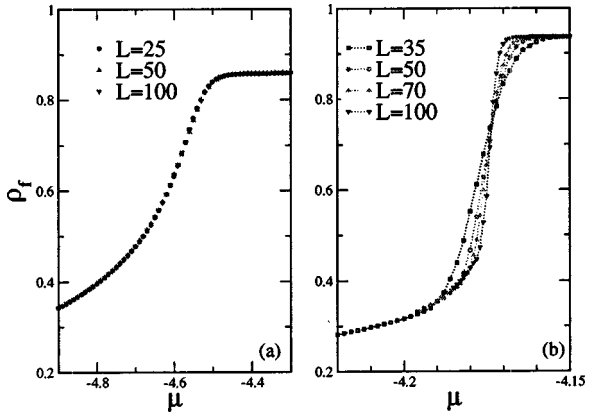

FIG. 19. Average equilibrium isotherms in 87% (a) and 95% (b) aerogels for different system sizes. The number of gel realizations ranges from 500 ($L=25$) to 20 ($L=100$) for the 87% aerogel and from 2000 ($L=35$) to 200 ($L=100$) for the 95% aerogel.

V. SUMMARY AND CONCLUSION

In this paper, we have proposed an interpretation of the hysteretic behavior observed in the experiments of ^{4}He adsorption in light silica aerogels. The overall shape of the experimental hysteresis loops is well described by our theoretical model and we have been able to reproduce the dramatic influence of porosity. In this interpretation, the disordered character of the aerogel structure plays an essential role, the porosity p being the tunable parameter that controls the amount of disorder in the system. The history-dependent behavior is thus associated with the presence of many metastable states in which the system may be trapped and that prevent thermal equilibration at low temperatures. The most important conclusion of our study is that adsorption and desorption obey to different mechanisms and may be gradual or discontinuous, depending on the porosity. Adsorption is insensitive to the presence of the interface between the solid and the external vapor, and the change in the shape of the isotherm from smooth to discontinuous as p increases from 87% to 95% has been related to the appearance of an infinite avalanche occurring in the bulk of the system, similar to what happens in the $T=0$ RFIM below the critical disorder [16]. In contrast, desorption is triggered by the presence of the outer surface and an associated depinning transition. The change in the shape of the isotherm is then related to a change in the morphology of the invading vapor domain from percolationlike to compact (note however that the mechanism may be different in aerogels of lower porosity [43]).

One must keep in mind that our calculations are based on local-mean-field theory in which disorder-induced fluctuations are properly accounted for but thermal fluctuations are neglected. This appears to be a reasonable assumption at very low temperatures where the time scale associated with thermally activated processes is much larger than the experimental time scale. In this case, both the adsorption and de-

sorption branches are metastable and we have shown that the true equilibrium isotherm (which probably cannot be reached experimentally) is somewhere in between: this isotherm also changes from gradual to discontinuous as p increases. The situation is different at higher temperature (in the vicinity of T_c) since true equilibrium behavior without hysteresis has been observed experimentally [2,4]. It will be of interest, therefore, to study the influence of temperature on the hysteretic behavior and to understand how the dynamics of relaxation towards equilibrium changes with T (see, e.g., Ref. [44] for a recent study of the relaxation behavior associated with capillary condensation in a lattice model of Vycor).

Finally, we suggest that the scenario for filling and draining described in this work could be tested in more detail by performing experiments in a series of aerogels of gradually increased porosity. If our interpretation of the adsorption process in terms of avalanches is correct, there should exist a value of the porosity for which the isotherm becomes critical and the distribution of avalanche sizes follows a power law with well-defined critical exponents [16]. Using superfluid instead of normal ^{4}He could perhaps allow us to observe distinct avalanche events in the aerogel and to study their statistical properties. Such a study has been performed recently in the nanoporous material nucleopore by a capacitance technique [45]. One could also check that the draining of the aerogel starts from the surface and that the growth of the invading vapor domain obeys different regimes. Related studies have been for instance carried out in Vycor using ultrasonic attenuation and scattering techniques [32,46]. Such experiments would give a definite answer to the long-standing question about the nature of hysteresis in fluid adsorption in disordered porous media.

ACKNOWLEDGMENTS

The Laboratoire de Physique Théorique des Liquides is the UMR 7600 of the CNRS. We thank R. Jullien for providing us with his lattice DLCA algorithm to build the model aerogel.

[1] F. Brochard and P.G. de Gennes, J. Phys. (France) Lett. **44**, L785 (1983); P.G. de Gennes, J. Phys. Chem. **88**, 6469 (1984).

[2] A.P.Y. Wong and M.H.W. Chan, Phys. Rev. Lett. **65**, 2567 (1990).

[3] L.B. Lurio, M. Mulders, M. Paerkau, M. Lee, S.G.J. Mochrie, and M.H.W. Chan, J. Low Temp. Phys. **121**, 591 (2000).

[4] A.P.Y. Wong, S.B. Kim, W.I. Goldburg, and M.H.W. Chan, Phys. Rev. Lett. **70**, 954 (1993).

[5] A.E. Bailey, B.J. Frisken, and D.S. Cannell, Phys. Rev. E **56**, 3112 (1997).

[6] See, e.g., D. P. Belanger in *Spin Glasses and Random Fields*, edited by A. P. Young (World Scientific, Singapore, 1998), p. 251.

[7] M.H.W. Chan, Czech J. Phys. Suppl. **S6**, 2915 (1996).

[8] D.J. Tulimieri, J. Yoon, and M.H.W. Chan, Phys. Rev. Lett. **82**, 121 (1999).

[9] It was recently reported, using a capacitive technique [J. R. Beamish and T. Herman, Physica B **329**, 340 (2003)], that hysteresis is present in the sorption isotherms of ^{4}He in a 95% porosity aerogel up to $T=5.155$ K and that the adsorption remained gradual at all temperatures below T_c. It is not yet clear whether these results, which challenge those of Ref. [2], are due to an insufficient equilibration of the system (very slow thermal relaxation in the coexistence region was indeed observed) or to a different preparation process of the aerogel. Hysteretic behavior in the same range of temperatures has also been found using a low-frequency mechanical oscillator [G. Gabay *et al.*, J. Low Temp. Phys. **121**, 585 (2000)].

[10] D. H. Everett, in *The Solid-Gas Interface*, edited by E. A. Flood (Marcel Dekker, New York, 1967), Vol. 2, p. 1055.

[11] P.C. Ball and R. Evans, Langmuir **5**, 714 (1989).

[12] We consider here hysteretic cycles that are observed at very slow flow rates on filling and on draining when the system exhibits no explicit time dependence (after some transient time). This corresponds to the so-called rate-independent limit.

[13] E. Kierlik, P.A. Monson, M.L. Rosinberg, L. Sarkisov, and G. Tarjus, Phys. Rev. Lett. **87**, 055701 (2001).

[14] E. Kierlik, P.A. Monson, M.L. Rosinberg, and G. Tarjus, J. Phys.: Condens. Matter **14**, 9295 (2002).

[15] M.L. Rosinberg, E. Kierlik, and G. Tarjus, Europhys. Lett. **62**, 377 (2003).

[16] J.P. Sethna, K. Dahmen, S. Kartha, J.A. Krumhansl, B.W. Roberts, and J.D. Shore, Phys. Rev. Lett. **70**, 3347 (1993); O. Perkovic, K. Dahmen, and J.P. Sethna, *ibid.* **75**, 4528 (1995); e-print cond-mat/9609072; K. Dahmen and J.P. Sethna, Phys. Rev. B **53**, 14 872 (1996); O. Perkovic, K. Dahnen, and J.P. Sethna, *ibid.* **59**, 6106 (1999).

[17] A. Berger, A. Inomata, J.S. Jiang, J.E. Pearson, and S.D. Bader, Phys. Rev. Lett. **85**, 4176 (2000); J. Marcos, E. Vives, L. Manosa, M. Acet, E. Duman, M. Morin, V. Novak, and A. Planes, Phys. Rev. B **67**, 224406 (2003).

[18] C.M. Soukoulis, K. Levin, and G.S. Grest, Phys. Rev. B **28**, 1495 (1983); H. Yoshizawa and D.P. Belanger, *ibid.* **30**, 5220 (1984); C. Ro, G.S. Grest, C.M. Soukoulis, and K. Levin, *ibid.* **31**, 1682 (1985); G.S. Grest, C.M. Soukoulis, and K. Levin, *ibid.* **33**, 7659 (1986); E.P. Raposo and M.D. Coutinho-Filho, *ibid.* **57**, 3495 (1998).

[19] See V. Krakoviack, E. Kierlik, M.L. Rosinberg, and G. Tarjus, J. Chem. Phys. **115**, 11 289 (2001) for a different treatment of liquid-vapor phase separation in aerogels using integral equation theory and the replica formalism in the continuum. This method, however, does not allow the study of the hysteretic behavior.

[20] H.-J. Woo, L. Sarkisov, and P.A. Monson, Langmuir **17**, 7472 (2001).

[21] K. Uzelac, A. Hasmy, and R. Jullien, Phys. Rev. Lett. **74**, 422 (1995); C. Vasquez, R. Paredes, A. Hasmy, and R. Jullien, Phys. Rev. Lett. **90**, 170602 (2003).

[22] R. Salazar, R. Toral, and A. Chakrabarti, J. Sol-Gel Sci. Technol. **15**, 175 (1999).

[23] E. Pitard, M.L. Rosinberg, G. Stell, and G. Tarjus, Phys. Rev. Lett. **74**, 4361 (1995).

[24] E. Kierlik, M.L. Rosinberg, G. Tarjus, and E. Pitard, Mol. Phys. **95**, 341 (1998).

[25] P. Meakin, Phys. Rev. Lett. **51**, 1119 (1983); M. Kolb, R. Botet, and R. Jullien, *ibid.* **51**, 1123 (1983).

[26] A. Hasmy, E. Anglaret, M. Foret, J. Pelous, and R. Jullien, Phys. Rev. B **50**, 6006 (1994).

[27] It is possible, however, that long-range correlations in the connectivity of the gel network exist that are not captured by the two-point function $g(r)$ [21]. This, for instance, may explain that no crossover to bulklike critical behavior is observed in the superfluid transition of ^{4}He in aerogel [J. Yoon *et al.*, Phys. Rev. Lett. **80**, 1461 (1998)].

[28] M. Lach-hab, A.E. Gonzalez, and E. Blaisten-Barojas, Phys. Rev. E **57**, 4520 (1998).

[29] G. Lawes, S.C.J. Kingsley, N. Mulders, and J. Parpia, Phys. Rev. Lett. **84**, 4148 (2000).

[30] J.V. Porto and J.M. Parpia, Phys. Rev. B **59**, 14 583 (1999).

[31] U. Marini Bettolo Marconi and F. van Swol, Phys. Rev. A **39**, 4109 (1989); A. Papadopoulou, F. van Swol, and U. Marini Bettolo Marconi, J. Chem. Phys. **97**, 6942 (1992).

[32] J.H. Page, J. Liu, B. Abeles, E. Herbolzheimer, H.W. Deckman, and D.A. Weitz, Phys. Rev. E **52**, 2763 (1995).

[33] A. I. Golov, I. B. Berkutov, S. Babuin, and D. J. Cousins, Physica B **329**, 258 (2003).

[34] F.J. Perez-Reche and E. Vives, Phys. Rev. B **67**, 134421 (2003).

[35] Strictly speaking, the disorder-induced critical transition studied by Sethna and co-workers [16] only exists at $T=0$. In LMFT, however, and more generally when thermal fluctuations can be neglected, this is again a well-defined transition and it is reasonable to assume that is characterized by the $T=0$ critical exponents. It is then easy to check that the finite-size scaling exponent χ identifies with the combination $\beta\delta/\nu$ of the exponents introduced in Ref. [16]. This is based on the hypothesis that close to p_c (for $p \geqslant p_c$) and $\mu_c=\mu_t(p_c)$ the discontinuous change in ρ_f is described by the scaling form $\Delta\rho_f(L,p,\mu)=r^\beta F_-(rL^{1/\nu},|h|/r^{\beta\delta})$, where $r=(p-p_c)/p_c$, $h=\mu-\mu_c$, and F_- is a universal scaling funtion. Defining a new universal scaling function $\tilde{F}_-(rL^{1/\nu},|h|L^{\beta\delta/\nu}) =(rL^{1/\nu})^\beta F_-(rL^{1/\nu},|h|/r^{\beta\delta})$, this can be rewritten as $\Delta\rho_f(L,p,\mu)=L^{-\beta/\nu}\tilde{F}_-(rL^{1/\nu},|h|L^{\beta\delta/\nu})$. Hence, $\partial\Delta\rho_f(L,p,\mu)/\partial\mu \propto L^{2-\eta}\partial\tilde{F}_-(rL^{1/\nu},|h|L^{\beta\delta/\nu})/\partial h$ with $2-\eta=(\beta\delta-\beta)/\nu$. According to Ref. [16], one has $1/\nu=0.71\pm0.09$, $\beta=0.035\pm0.028$, $\beta\delta=1.81\pm0.32$, and $\eta=0.73\pm0.28$. Note that in Fig. 11, we have neglected the dependence on the distance to p_c and used $\chi=\beta\delta/\nu\simeq 2-\eta$. In fact, according to Ref. [34], the scaling behavior of the magnetization jump in the $T=0$ RFIM could be more complicated than the one predicted by Sethna and co-workers.

[36] B. Tadic, Phys. Rev. Lett. **77**, 3843 (1996).

[37] M. Cieplak and M.O. Robbins, Phys. Rev. Lett. **60**, 2042 (1988).

[38] See, e. g., B. Koiller and M.O. Robbins, Phys. Rev. B **62**, 5771 (2000), and references therein.

[39] In the absence of gel, there is no threshold for the onset of motion of the initial liquid-vapor interface parallel to the [100] plane of the bcc lattice, i.e., the interface moves along the x axis for $\mu<\mu_{sat}=-4$ at all temperatures. The actual self-affine interface, however, has various orientations at short-length scale. We found numerically that, at $T/T_c=0.45$, a portion of the interface parallel to the [110] plane starts to move at $\mu=-4.11$. Since the drop in the desorption isotherms of Fig. 12 occurs at lower values of μ, the pinning of the interface is due to disorder and not to lattice effects.

[40] H. Ji and M.O. Robbins, Phys. Rev. B **46**, 14 519 (1992).

[41] In the thermodynamic limit, the boundary condition (presence or absence of an interface) is not expected to influence the equilibrium phase behavior in the bulk of the material. As we have seen before, this reasoning does not apply to metastable states and out-of-equilibrium behavior.

[42] The presence of a jump in the adsorption isotherm also implies that there are no adsorption scanning curves in the upper part of the hysteresis loop. Indeed, in the absence of interface with the reservoir, these curves are obtained by readsorbing from the metastable states located along the last desorption scanning curve.

[43] F. Detcheverry, E. Kierlik, M. L. Rosinberg, and G. Tarjus (unpublished).

[44] H.-J. Woo and P.A. Monson, Phys. Rev. E **67**, 041207 (2003).

[45] M.P. Lilly and R.B. Hallock, Phys. Rev. B **64**, 024516 (2001); M.P. Lilly, A.H. Wootters, and R.B. Hallock, *ibid.* **65**, 104503 (2002).

[46] E.S. Kikkinides, M.E. Kainourgiakis, K.L. Stefanopoulos, A.Ch. Mitropoulos, A.K. Stubos, and N.K. Kanellopoulos, J. Chem. Phys. **112**, 9881 (2000).